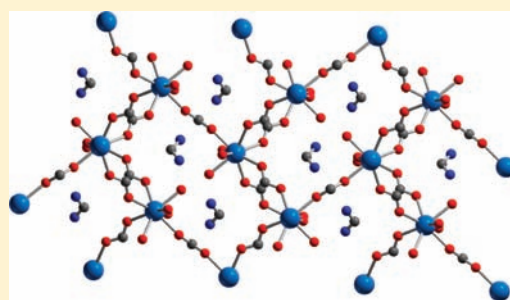


Amine-Templated Polymeric Lanthanide Formates: Synthesis, Characterization, and Applications in Luminescence and Magnetism

Andrea Rossin,^{*,†} Giuliano Giambastiani,[†] Maurizio Peruzzini,^{*,†} and Roberta Sessoli[‡][†]Consiglio Nazionale delle Ricerche, Istituto di Chimica dei Composti Organometallici (ICCOM-CNR), Via Madonna del Piano 10, 50019 Sesto Fiorentino (Firenze), Italy[‡]Dipartimento di Chimica "Ugo Schiff" & INSTM, Università degli Studi di Firenze, Via della Lastruccia 3, 50019 Sesto Fiorentino (Firenze), Italy

Supporting Information

ABSTRACT: The novel polymeric formates of general formula $[(\text{Fmd})\text{-Ln}^{\text{III}}(\text{HCOO})_4]_{\infty}$ ($\text{Fmd}^+ = \text{NH}_2\text{-CH}^+\text{-NH}_2$; $\text{Ln} = \text{Eu}$ (1), Gd (2), Tb (3), Dy (4)) were synthesized through solvothermal methods in formamide solutions. The compounds are isostructural; they crystallize in the orthorhombic $C222_1$ chiral space group. The coordination geometry at the metal centers is square antiprismatic (coordination number eight), with each formate ligand bridging adjacent lanthanide ions. The overall negative three-dimensional (3D) framework charge is balanced by the formamidinium cations sitting inside the channels along the a axis, forming extensive $\text{N}\cdots\text{H}\cdots\text{O}$ hydrogen bonding with the surrounding cage. All the compounds have been characterized through single-crystal/powder X-ray diffraction, IR spectroscopy, and TG-MS analysis. Finally, their luminescence and magnetic properties have been assessed, leading to remarkable emission intensities, especially for the $\text{Tb}(\text{III})$ compound ($\Phi = 0.83$), with corresponding lifetime decays in the micro (Dy) and millisecond (Tb , Eu) time scale. A weak but sizable antiferromagnetic interaction has been observed for the $\text{Gd}(\text{III})$ derivative.



INTRODUCTION

Trivalent lanthanide ions are fascinating luminescence sources, owing to their high color purity and relatively long lifetimes associated to the 4f-shell electronic transitions.¹ They have attracted interest in a wide range of important electronic and biotechnological fields.² For instance, emitting complexes of $\text{Tb}(\text{III})$ and $\text{Eu}(\text{III})$ ions are employed as markers in fluoroimmunoassays,³ where a quantitative estimation of antigens in biological matrixes is needed. Because of their strong and long-lived luminescence, the background signal from the biological matrix can be circumvented making the detection of the desired analytical signal particularly easy.⁴ Moreover, a new-generation of in vivo imaging technologies requires low-frequency light because of its penetration capability through biological tissues. To this end, NIR luminescence from $\text{Yb}(\text{III})$, $\text{Nd}(\text{III})$, $\text{Pr}(\text{III})$, $\text{Er}(\text{III})$ and related complexes are particularly attractive.⁵ Other relevant practical applications where $\text{Ln}(\text{III})$ ions may be involved are related to the optical amplification in laser technology [$\text{Nd}(\text{III})$] or to the production of silica-based fibers for optical networks, where the emission wavelengths of $\text{Pr}(\text{III})$ (ca. 1330 nm) and $\text{Er}(\text{III})$ (ca. 1550 nm) ions closely match with the "windows of transparency" in silica used for telecommunications.⁶ Lanthanide-Organic Frameworks (LOFs) are an emerging class of materials, whose practical applications in the fields of sensing, catalysis, magnetism, and luminescence are steadily widening.⁷ The hybrid nature of LOFs, being formed by an organic ligand and a metal ion within a (typically)

porous structure, enables a wide range of emissive phenomena, such as linker-based luminescence,⁸ metal-based emission⁹ or antennae effects.¹⁰ Both the inorganic and the organic moieties can provide the platforms to generate luminescence, while metal–ligand charge transfer related luminescence within Metal-Organic Frameworks (MOFs) can add further luminescent functionalities. Furthermore, some guest molecules reversibly adsorbed within MOF pores can also emit and/or induce luminescence. The permanent porosity of some MOFs has enabled their reversible storage and release of luminescent guest substrates and provided the hosts for their differential recognitions with sensing species.

As far as magnetism is concerned,¹¹ the response to external magnetic stimuli (magnetic fields) can be strongly enhanced by the incorporation of magnetic moment carriers like paramagnetic metal ions or/and open-shell organic ligands. Lanthanides play a key role in magnetism, some of them exhibiting very large magnetic moments and very strong magnetic anisotropy. However, networks based on trivalent lanthanide ions, thus containing unpaired electrons only in the well shielded 4f orbitals, are characterized by very weak exchange interactions and very low transition temperatures to bulk magnets.¹² Nevertheless, the strong magnetic anisotropy is sufficient to give rise to slow relaxation of the magnetization in

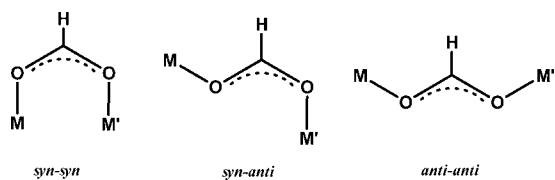
Received: April 26, 2012

Published: June 5, 2012

the paramagnetic phase,¹³ with the opening of hysteresis above liquid helium temperature as in the case of Single Molecule Magnets (SMMs) based on Tb(III) phthalocyaninate complexes.¹⁴ A similar behavior is also observed in lanthanide based extended one-dimensional structures,¹⁵ known as Single Chain Magnets,¹⁶ where both magnetic anisotropy and exchange interactions contribute to freeze the magnetic moments. A short connection between the magnetic centers is however necessary to provide significant interactions.

Carboxylic acids are the most popular organic spacers employed for LOFs construction, because of the high lanthanide ions affinity for oxygen. Short and rigid carboxylates like oxalate⁷ or formate⁷ are particularly useful to get well-defined three-dimensional (3D) architectures. The latter in particular shows a versatile coordination mode, acting as a monodentate, chelating or bridging spacer in *syn-syn*, *syn-anti*, or *anti-anti* configuration (Scheme 1). In addition, the small

Scheme 1. Possible Coordination Modes of the μ -HCOO⁻ Ligand



linker size makes it suitable for the synthesis of network exhibiting bulk magnetic properties. In particular Mn(HCOO)₃ has been found to order magnetically around 20 K.¹⁷

Following our recent interest for the synthesis of polymeric metal formates,¹⁸ we prepared four new materials of general formula [(Fmd)Ln^{III}(HCOO)₄]_∞ (Fmd⁺ = NH₂-CH⁺-NH₂; Ln = Eu (1), Gd (2), Tb (3), Dy (4)). The compounds are isostructural, and they have been typically characterized through solid-state techniques (single-crystal and powder X-ray diffraction, IR spectroscopy, TG-MS analysis). Their luminescence (for 1, 3, and 4) and magnetic (for 2 and 4) properties were finally assessed. 1, 3, and 4, upon excitation with UV light, showed typical metal-centered (MC) emission bands in the visible range (red, green, and blue-greenish, respectively) with remarkable emission intensity, especially for the Tb(III) derivative 3. Long lifetime decays, in the micro (Dy) and millisecond time scale (Eu, Tb), have also been measured. The formate ligand has been found to transmit a weak antiferromagnetic interaction between Gd(III) centers in 2. In the case of 3 and 4, the magnetic behavior is dominated by the depopulation of the crystal field split levels of the ⁷F₆ and ⁶H_{15/2} multiplets of Tb(III) and Dy(III), respectively. No significant slow relaxation of the magnetization is however observed.

EXPERIMENTAL SECTION

Materials and Methods. All starting materials and solvents were of analytical grade. They were purchased from Aldrich and used as received, without further purification. Single crystal X-ray data of 4 were collected at ambient temperature (298 K) on an Oxford Diffraction XCALIBUR 3 diffractometer equipped with a CCD area detector using Mo K α radiation ($\lambda = 0.7107$ Å). The program used for the data collection was CrysAlis CCD 1.171.¹⁹ Data reduction was carried out with the program CrysAlis RED 1.171²⁰ and the absorption correction was applied with the program ABSPACK 1.17. Direct methods implemented in Sir97²¹ were used to solve the structures and

the refinements were performed by full-matrix least-squares against *F*² implemented in SHELX97.²² All the non-hydrogen atoms were refined anisotropically while the hydrogen atoms of the formate ligands were fixed in calculated positions and refined isotropically with the thermal factor depending on the one of the carbon atom to which they are bound. The Fmd⁺ N-hydrogens were located on the Fourier difference density maps and refined isotropically with the thermal factor depending on those of the nitrogens to which they are bound. The geometrical calculations were performed by PARST97,²³ and molecular plots were produced by the program ORTEP3.²⁴ X-ray powder diffraction (XRPD) measurements were carried out with a Panalytical X'PERT PRO powder diffractometer equipped with a diffracted beam Ni filter and an PIXcel solid state detector in the 4–60° 2 θ region, operating with CuK α radiation ($\lambda = 1.54$ Å). Antiscatter slits were used both on the incident (0.25° and 0.5° divergence) and the diffracted (7.5 mm height) beam. Variable temperature (VT) X-ray powder diffraction patterns were collected in the 25–450 °C temperature range using an Anton Paar HTK 1200N Oven camera. The measurements were carried out at ambient pressure under a mild N₂ flow, at a heating rate of 10 °C min⁻¹. Thermal gravimetric analysis measurements were performed on an EXSTAR Thermo Gravimetric Analyzer (TG/DTA) Seiko 6200 under N₂ atmosphere (100 mL min⁻¹). IR spectra were recorded on KBr pellets in the 4000–400 cm⁻¹ range. The C, H, N elemental analyses were made at ICCOM-CNR using a Thermo FlashEA 1112 Series CHNS-O elemental analyzer with an accepted tolerance of ± 0.4 units on carbon (C), hydrogen (H), and nitrogen (N). The (powdered) solid state samples were placed in between two quartz disks fixed by a dedicated metal pincer. Uncorrected emission spectra were obtained with an Edinburgh FLS920 spectrometer equipped with a peltier-cooled Hamamatsu R928 photomultiplier tube (185–850 nm). An Edinburgh Xe900 450 W xenon arc lamp was used as exciting light source. Corrected spectra were obtained through a calibration curve supplied with the instrument. The luminescence lifetimes in the μ s-msec scales were measured by using a Perkin-Elmer LS-50 spectrofluorimeter equipped with a pulsed xenon lamp with variable repetition rate and elaborated with standard software fitting procedures. The photoluminescence quantum yields have been calculated through corrected emission spectra obtained from an apparatus consisting of a barium sulfate coated integrating sphere (4 or 6 in.), a He–Cd laser (λ_{exc} : 325 nm, 5mW) or a 450W Xe lamp (with a λ_{exc} tunable by a monochromator supplied with the instrument) as light sources, and a R928 photomultiplier tube or a CCD AVA-Spec2048 as signal detectors, following the procedure described by De Mello et al.²⁵ Experimental uncertainties are estimated to be $\pm 8\%$ for lifetime determination, $\pm 20\%$ for emission quantum yield, ± 2 nm and ± 5 nm for absorption and emission peaks, respectively.

The magnetic properties were measured on microcrystalline powders pressed in a pellet to avoid preferential orientation of the crystallites because of magnetic torque. The field dependence of the magnetization and the temperature dependence of the static susceptibility of 2, 3, and 4, estimated from the *M/H* ratio, was measured in *H* = 1 kOe in the 2–35 K temperature range and in *H* = 10 kOe for higher temperature by using a Quantum Design MPMS Squid magnetometer. The alternating current (ac) susceptibility in the frequency range 0.1 Hz–1 kHz was measured with the same equipment. Higher frequencies have been measured with a Quantum Design PPMS platform.

Preparation of [(Fmd)Ln(HCOO)₄]_∞. The preparation is the same for all the lanthanides considered. Only the synthesis of the Dy(III) derivative 4 is described here as a representative example. Dysprosium(III) nitrate hexahydrate [Dy(NO₃)₃·6H₂O, 1.95 g, 5.6 mmol] and cyclobutane-1,1'-dicarboxylic acid (0.40 g, 2.8 mmol) were dissolved in 10 mL of formamide. The clear solution was transferred to a Teflon-lined stainless steel autoclave (inner Teflon beaker volume ca. 15 mL), sealed and heated at 130 °C for 24 h under autogenous pressure. After slow overnight cooling, colorless crystals of 4 were collected, washed with ethanol (4 × 10 mL), petroleum ether (4 × 10 mL), and finally dried under a nitrogen stream at room temperature. Yield: 1.04 g [48%, calculated with respect to the Dy(III) salt]. The

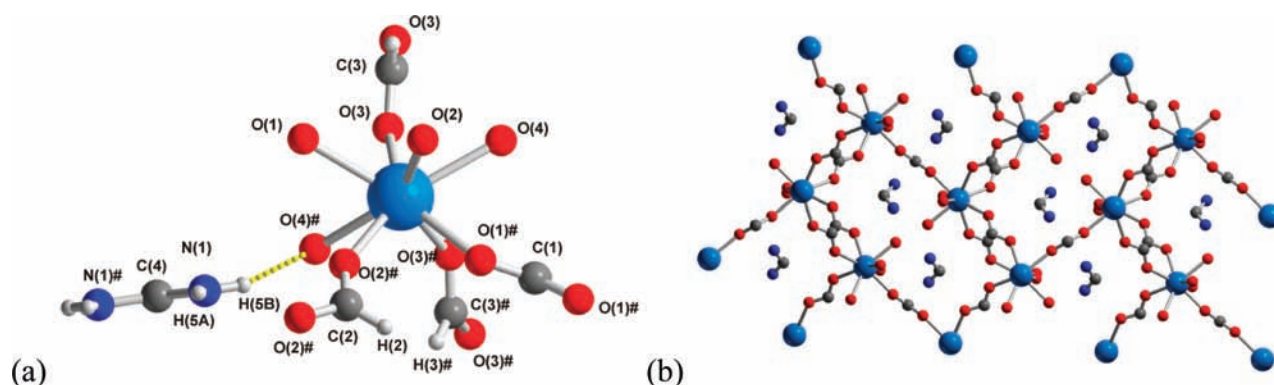


Figure 1. (a) Unit cell of the crystal structure of **4** and (b) view of the polymer channels along the *a* axis. In (b), H atoms on the scaffold are omitted for clarity. Atom color code: light blue, Dy; gray, C; white, H; red, O; blue, N. Hydrogen bonds depicted in yellow dotted lines.

phase purity was checked through XRPD, comparing the experimental diffractogram with that calculated from the single-crystal structure (Supporting Information, Figure S1). Anal. Calcd. for **4**, $C_5H_9DyN_2O_8$ (388.97): C, 15.49; H, 2.34; N, 7.23. Found: C, 15.56; H, 2.42; N, 7.38. IR bands (KBr, cm^{-1}) for **4**: 2846 m [$\nu(C-H)$ formate]; 1720 s and 1602 vs [$\nu(COO^-)$]; 1384 s [$\nu(C-N)$], 1333 m, 1120 w, 1065 w, 801 s [$\gamma(C-H)$], 732 m, 533 w.

Ln = Eu (1). The starting salt used was Europium(III) nitrate hydrate [$Eu(NO_3)_3 \cdot xH_2O$]. Yield: 1.27 g (61%, based on Europium). See Supporting Information, Figure S2 for the XRPD pattern of **1**. Anal. Calcd. for **1**, $C_5H_9EuN_2O_8$ (377.96): C, 15.93; H, 2.41; N, 7.43. Found: C, 16.06; H, 2.27; N, 7.59. IR bands (KBr, cm^{-1}) for **1**: 2840 m [$\nu(C-H)$ formate]; 1722 s and 1602 vs [$\nu(COO^-)$]; 1384 s [$\nu(C-N)$], 1332 m, 1119 w, 1064 w, 790 s [$\gamma(C-H)$], 730 m, 533 w.

Ln = Gd (2). The starting salt used was Gadolinium(III) nitrate hexahydrate [$Gd(NO_3)_3 \cdot 6H_2O$]. Yield: 1.63 g (77%, based on Gadolinium). See Supporting Information, Figure S3 for the XRPD pattern of **2**. Anal. Calcd. for **2**, $C_5H_9GdN_2O_8$ (382.39): C, 15.70; H, 2.37; N, 7.33. Found: C, 15.43; H, 3.52; N, 7.61. IR bands (KBr, cm^{-1}) for **2**: 2843 m [$\nu(C-H)$ formate]; 1714 s and 1603 vs [$\nu(COO^-)$]; 1368 s [$\nu(C-N)$], 1119 w, 1064 w, 792 s [$\gamma(C-H)$], 728 m, 534 w.

Ln = Tb (3). The starting salt used was Terbium(III) nitrate hexahydrate [$Tb(NO_3)_3 \cdot 6H_2O$]. Yield: 1.84 g (77%, based on Terbium). See Supporting Information, Figure S4 for the XRPD pattern of **3**. Anal. Calcd. for **3**, $C_5H_9TbN_2O_8$ (383.96): C, 15.64; H, 2.36; N, 7.29. Found: C, 15.93; H, 2.30; N, 6.96. IR bands (KBr, cm^{-1}) for **3**: 2845 m [$\nu(C-H)$ formate]; 1722 s and 1599 vs [$\nu(COO^-)$]; 1384 s [$\nu(C-N)$], 1120 w, 1064 w, 792 s [$\gamma(C-H)$], 729 m, 534 w.

RESULTS AND DISCUSSION

Synthesis and Structure. The solvothermal synthesis of amine-templated polymeric formates through an acid-catalyzed solvent hydrolysis has been successfully employed by our research group in the case of magnesium as the metal center.¹⁸ The extension of this experimental protocol to rare earths led to the preparation of the analogous species of general formula $[(Fmd)Ln^{III}(HCOO)_4]_{\infty}$ [$Ln = Eu$ (**1**), Gd (**2**), Tb (**3**), Dy (**4**)], where the central trivalent ion shows coordination number eight instead of six (cf. $[(Fmd)Mg(HCOO)_3]_{\infty}$).^{18,26} The starting lanthanide salt does not seem to influence the reaction outcome: the same product is obtained when starting from either $Ln(NO_3)_3$ or $LnCl_3$, as confirmed by the comparison of the corresponding XRPD patterns. The isostructural compounds **1–4** crystallize in the orthorhombic (chiral) $C22_1$ space group. Chirality is generated by the helicoidal packing of the bridging formate ions combined with a square antiprismatic coordination geometry around the lanthanide ion (Figure 1). The resulting 3D network bears a negative charge that is balanced by the formamidinium cation

lying inside the polymer channels. As explained previously, Fmd^+ is generated by the controlled hydrolysis of the formamide solvent under the (mildly) acidic reaction conditions.²⁶ The $-NH_2$ groups of Fmd^+ engage into bifurcate $N-H \cdots O$ hydrogen bonding with the surrounding formates (Table 1), thus providing considerable framework robustness.

Table 1. Hydrogen Bonds for **4 [\AA and deg]^a**

D–H \cdots A	<i>d</i> (D–H)	<i>d</i> (H \cdots A)	<i>d</i> (D \cdots A)	\angle (DHA)
N(1)–H(SA) \cdots O(1)#7	0.86	2.24	3.038(7)	155.0
N(1)–H(SB) \cdots O(4)	0.86	2.20	3.000(7)	155.0
N(1)–H(SB) \cdots O(2)	0.86	2.47	3.092(8)	130.1

^aSymmetry transformations used to generate equivalent atoms: #1 $-x+1, y, -z+1/2$; #2 $x, -y+2, -z+1$; #3 $-x-1/2, -y+3/2, z-1/2$; #4 $-x-1, y, -z+3/2$; #5 $-x-1/2, -y+3/2, z+1/2$; #6 $-x, y, -z+1/2$; #7 $-x, -y+2, z+1/2$.

The compounds isostructurality was confirmed through the comparison of their XRPD patterns (Supporting Information, Figures S1–S4) whose peaks only show a small 2θ variation related to the (slightly) different Ln^{3+} ion size. Their networks belong to the $ecu(3^6 \cdot 4^{15} \cdot 5^7)$ rare topology²⁷ (determined using the TOPOS free software package,²⁸ with Ln^{III} nodes and $HCOO^-$ connections), the same as those found for the structurally related Erbium-based $\{(dmenH_2)[Er(HCOO)_4]_2\}_{\infty}$ ($dmenH_2 = N,N'$ -dimethylethylenediammonium)²⁹ and $[(Fmd)Er(HCOO)_4]_{\infty}$ ³⁰ frameworks. Single crystal X-ray diffraction was performed only on **4**. Thus, only a brief comment on the structural features related to the Dy(III) derivative will be made in here. The main bond distances and angles [$d(Dy-O)_{ave} = 2.37 \text{ \AA}$; $d(C-N) = 1.283(6) \text{ \AA}$; $\alpha(O-Dy-O)_{ave} = 77.7^\circ$] fall in the ordinary range observed for other similar species.³¹ The formate ligands [$d(C-O)_{ave} = 1.24 \text{ \AA}$; $\alpha(O-C-O)_{ave} = 125.4^\circ$] are bridging the metal centers in an *anti-anti* conformation. See the Supporting Information, Tables S1–S4 for the complete crystallographic data set.

Thermal Behavior. The TG-MS analyses of **1–4** again showed a very similar behavior (see Figure 2 for the case of **2**, chosen as a representative example. See the Supporting Information, Figures S8, S10, and S11 for the TG-MS plots of **1**, **3**, and **4**, respectively). The thermal behavior of **2** can be summarized as follows: formation of an intermediate $Gd(HCOO)_3$ phase in the 250–320 °C temperature range [weight loss = 23.8% (calculated); 23.6% (experimental)] after both formamide and formic acid loss {analogously to

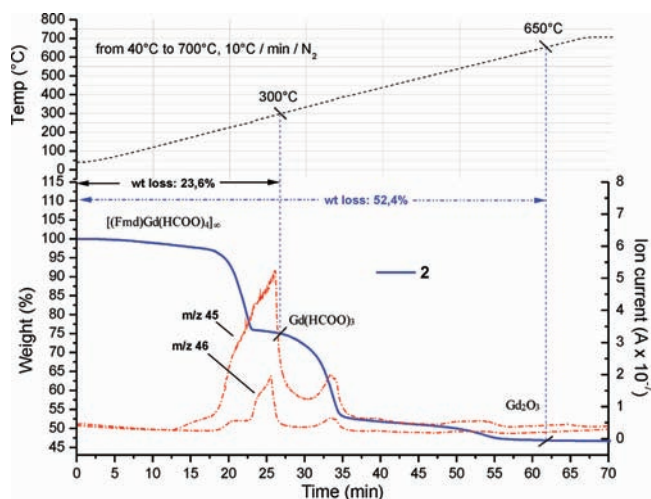


Figure 2. TG-MS profile for **2**. See the Supporting Information, Figure S9 for the corresponding weight loss (%) versus temperature graph.

what was observed for $[(\text{Fmd})\text{Mg}(\text{HCOO})_3]_\infty$,²⁶ which in turn releases CO and H₂O leading to the corresponding Gd₂O₃ oxide above 600 °C [total weight loss = 52.7% (calculated); 52.4% (experimental)].

The identity of the intermediate phase was assessed through variable-temperature powder X-ray diffraction (Figure 3). The peaks appearing on the XRPD diffractogram of **2** at 250 °C are coincident with those coming from a pure Gd(HCOO)₃ sample prepared in an independent synthesis from Gadolinium(III) carbonate and formic acid (Supporting Information, Figures S5 and S7).³² The structure of anhydrous gadolinium formate has already been solved from powders:³³ its crystal system is trigonal (space group *R3m*), with triangular channels along the *c* axis (Supporting Information, Figure S6). The compound is isomorphous to the neodymium,³⁴ praseodymium,³⁴ samarium,³⁵ and cerium³⁶ analogues. Further heating generates an amorphous phase in the 350–600 °C range, from which cubic gadolinium oxide Gd₂O₃³⁷ crystallizes at temperatures above 600 °C.

Luminescence Properties. Owing to their low molar extinction coefficients, Ln(III) ions are normally matched with π -conjugated multidentate organic chromophores (antennae)

within LOFs, to enhance the harvested light to be transferred to the emitting metal levels.³⁸ In the present case, since the small formate linker cannot generate any antenna effect, a direct excitation (365 nm) of the Ln(III) ion absorption bands was necessary. On the other hand, in these polymeric formates the photoluminescence efficiency was found to be remarkably high, because of the lack of intermediate processes (photoinduced energy transfer). Figure 4 shows the emission spectra of **1**, **3**,

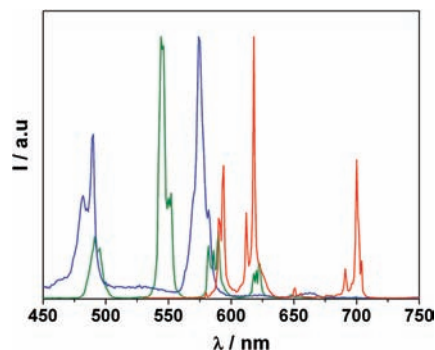


Figure 4. Room temperature normalized emission spectra ($\lambda_{\text{exc}} = 365$ nm) of **1** (red line), **3** (green line) and **4** (blue line).

and **4** in the solid state (as powders). The line-like bands, typical of trivalent lanthanide ions, originate from internal f-f transitions (shielded by both 5s and 5p subshells).³⁹ The Dy(III) ion emission bands at 490 and 574 nm are related to the $^4\text{F}_{9/2} \rightarrow ^6\text{H}_{15/2}$ and $^4\text{F}_{9/2} \rightarrow ^6\text{H}_{13/2}$ transitions, while Eu(III) and Tb(III) multiple lines arise from $^5\text{D}_1, ^5\text{D}_0 \rightarrow ^7\text{F}_j$ and $^5\text{D}_4 \rightarrow ^7\text{F}_j$ ones, respectively.^{2a} The corresponding strong emission intensities, especially for the Tb-containing compound (**3**, $\Phi_{\text{em}} = 0.83$), are clearly visible to the naked eye. The related lifetime decays span from the micro- (**4**) to the millisecond (**1,3**) time scale (see Table 2).

The optical features of the Tb(III)-containing network **3** have been investigated on a ITO (Indium–Tin Oxide) substrate. The supported material has been prepared through deposition from solvothermal mother solutions,⁴⁰ by merging an ITO-coated glass plate into the reagents solution at the bottom of the Teflon beaker used for the ordinary synthesis of **3**; the crystals of the LOF were deposited on the support

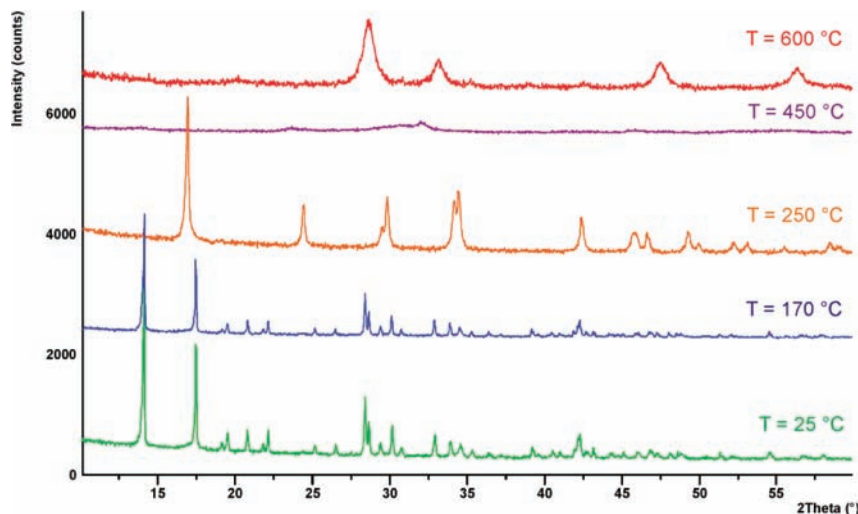


Figure 3. VT-XRPD diffractograms of **2**.

Table 2. Photophysical Properties of 1, 3, and 4 in the Solid State (Room Temperature)

	$\lambda_{\text{max}}/\text{nm}$	Φ_{em}^a	$\tau/\mu\text{s}$
1	594–618–700	0.25	1.7×10^3
3	492–544–590–624	0.83	2.0×10^3
4	490–574	<i>b</i>	2.1

^a λ_{exc} : 365 nm. ^bNot measured because of signal weakness.

during their formation at high temperature. Although the film obtained was not homogeneous and the photoluminescence quantum yield (PLQY) could not be detected (the shape of the sample does not fit the integrating sphere sample holder), the lifetime was identical to that of the powder sample (2.1 ms). Given the close correlation between the lifetime and the PLQY for Ln(III) ions,⁴¹ it can be stated that the photoluminescence properties of the network are not (or negligibly) affected by the environment, providing thereby an opening to a larger number of application fields.

Magnetic Properties. The temperature dependence of the $\chi_{\text{M}}T$ product of the paramagnetic samples 2, 3, and 4 is reported in Figure 5. Given that exchange interactions are

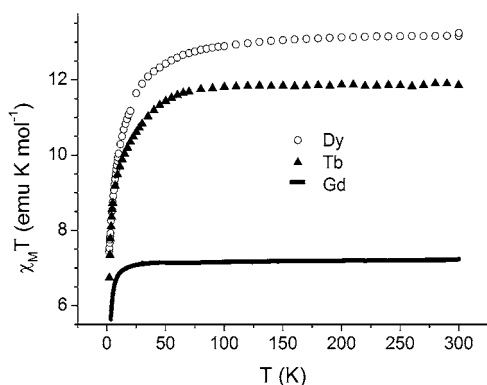


Figure 5. Temperature dependence of the product of the magnetic susceptibility with temperature of 2 (thick line), 3 (solid triangles), and 4 (empty circles).

expected to be weak and play a role only at very low temperatures, the magnetic properties of 1 (which is characterized by a non magnetic 7F_0 state) have not been investigated. The room temperature value of $\chi_{\text{M}}T$ of 2, 7.24 emu K mol⁻¹, is close to that expected for an isolated $S = 7/2$ with $g = 2$, 7.875 emu K mol⁻¹, taking also into account the hygroscopic nature of the compound and that no treatment has been performed before the measurements. On decreasing the temperature below 30 K, a monotonic decrease is observed, suggesting the presence of antiferromagnetic interactions. Given the 3D nature of the network the data have been analyzed using the Curie–Weiss law by plotting χ^{-1} versus T (Supporting Information, Figure S12). A linear fit of the data provided the Curie constant, 7.25 emu K mol and $\theta = -0.54$ K. Thus, the magnetic interaction mediated by the formate ligand is weak but sizable and antiferromagnetic in nature, comparable to that found in a diphosphonate based 3D network.⁴²

The magnetic behavior of 3 and 4 is more complex. The room temperature value of 3, 11.9 emu K mol⁻¹, is in reasonable agreement with that expected for the $J = 6$ with $g_{\text{J}} = 3/2$, which characterize the 7F_6 state of Tb(III), 11.82 emu K mol⁻¹. Similarly, the room temperature value, 13.2 emu K

mol⁻¹, is in good agreement with that expected for the $J = 15/2$ with $g_{\text{J}} = 4/3$ of the ${}^6H_{15/2}$ state of Dy(III), 14.17 emu K mol⁻¹. In both cases, a decrease of $\chi_{\text{M}}T$ occurs at a higher temperature than that of 2, but this phenomenon can be ascribed to the gradual depopulation of the highest level of the 7F_6 and ${}^6H_{15/2}$ multiplets of 3 and 4, respectively, because of crystal effects rather than magnetic exchange. The overall splitting is in fact several hundreds of K, as confirmed by the width and complex structure of the ${}^5D_4 \rightarrow {}^7F_6$ and ${}^4F_{9/2} \rightarrow {}^6H_{15/2}$ bands around 480 nm of the luminescence spectrum of 3 and 4 (see Figure 4). An estimation of the exchange interaction is therefore not possible in this case. This interpretation is further confirmed by the analysis of the magnetization versus field curves recorded for 3 and 4 at different temperatures in the range 2–10 K (see Supporting Information, Figure S13). These curves do not rescale on a single curve when plotted versus the reduced H/T variable and do not show saturation at low temperature due to the strong magnetic anisotropy.

To investigate the dynamic behavior of the magnetization of these extended structures, the susceptibility in an ac field^{12,13} of 2, 3, and 4 has been measured in zero static field (Supporting Information, Figures S14–S16), but no frequency dependence or a significant imaginary component of the susceptibility has been observed, suggesting that the zero field relaxation is faster than the employed frequencies also at the lowest investigated temperature (2 K). The application of a static field has often been employed to suppress a fast relaxation mechanism.¹³ The frequency dependence of the ac susceptibility has thus been measured by varying the static field. A significant difference is observed among the three compounds. In fact, 2 exhibits at 10 K a significant frequency dependent imaginary component, which is not the case of 3 at any temperature down to 2 K, while a weak imaginary component is observed for 4 at the lowest temperature. The temperature dependence of the imaginary component (χ'') of 2 measured in a static field of 2 kOe is reported in Figure 6. The related graph for the real component χ' is shown in Supporting Information, Figure S17. The data analysis using the Debye model¹³ has allowed to extract the temperature dependence of the relaxation, shown as an Arrhenius plot in the inset of Figure 6. A thermally activated regime is observed above 5 K, and the highest investigated temperatures provide for the Arrhenius law $\tau = \tau_0 \exp(\Delta/k_{\text{B}}T)$

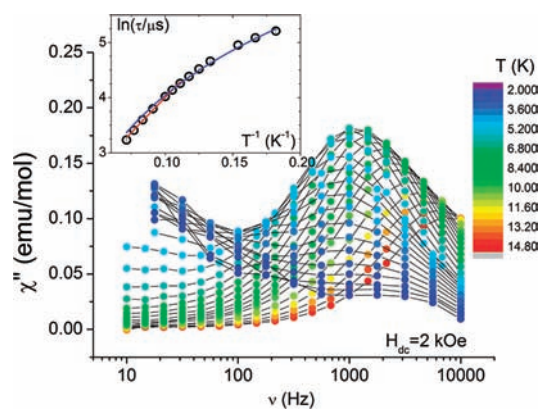


Figure 6. Temperature dependence of the magnetization imaginary component of 2 measured in a static field. In the inset, the temperature dependence of the relaxation time. The red and blue lines correspond to the best fit through either an exponential (Arrhenius) or a polynomial function, respectively.

the following parameters: $\tau_0 = 4.2(3) \times 10^{-6}$ s, $\Delta = 25(1)$ K (red line in the inset of Figure 6). The relaxation time seems, however, to level off at lower temperatures, but below 5 K the χ'' versus ν curves become too distorted to extract a relaxation time, and a decreasing fraction of the magnetization is involved in the monitored relaxation process. In these extended structures, the slower magnetic relaxation (although in applied static fields) is observed for the most isotropic lanthanide ion, Gd(III). This trend is opposite to that observed in discrete molecules showing magnetic bistability, also known as Single Molecule Magnets, while is rather common in traditional paramagnets. Indeed, a similar slow relaxation in static field was previously observed in another extended network of Gd(III) ions linked by fumarate ligands.⁴³ In that case, the analysis of the temperature dependence of the relaxation time was performed assuming a $\tau = aT^n$ dependence. The slow relaxation was not attributed to an anisotropy barrier, but to the phonon-bottleneck effect originated by the trapping of resonant phonons that are unable to release the energy of the spin bath to the thermal one.⁴⁴ A similar analysis performed on **2** provides a better agreement with the experimental data (see blue line in the inset of Figure 6) and a best fit value $n = -2.0(1)$. An exponent equal to -2 is theoretically expected for this phonon-bottleneck phenomenon. The observation of this phenomenon in two different Gd-MOF structures suggests that the coordinative 3D network can play a role in trapping resonant phonons.

CONCLUSIONS

Four novel polymeric lanthanide formates of general formula $[(\text{Fmd})\text{Ln}^{\text{III}}(\text{HCOO})_4]_{\infty}$ have been prepared through solvothermal methods. The isomorphous species show an amine-templated 3D polymeric lattice, whose luminescence and magnetic properties have been assessed. The compounds containing Dy(III), Eu(III), and Tb(III) showed remarkable emission intensity (Φ_{em} up to 0.83) and long lifetime decays in the micro- (Dy) and millisecond (Tb, Eu) time scale. Their photoluminescence features were not affected by changing the environment (i.e., by growing crystals of the material on an ITO-coated support). The magnetic investigation revealed the unambiguous presence of weak antiferromagnetic interaction between Gd(III) ions. While the Tb(III) and Dy(III) analogues, despite their significant orbital contributions, do not show the slow relaxation that characterize Single Molecule or Single Chain Magnets, a temperature dependent mechanism of relaxation is observed for the Gd(III) derivative in static applied fields. Weakly coupled Gd(III) systems are particularly interesting for their large magnetocaloric effect⁴⁵ exploitable in refrigerators based on the adiabatic demagnetization process. Examples of extended systems exploited for this purpose are scarce.⁴⁶ To be usable as refrigerants, the magnetization dynamics of these materials must be fast compared to the field ramp. This appears to be the case for **2**, whose relaxation time is in the milliseconds range. While the characterization of the magnetocaloric properties of these compounds is in progress, controlled change of their physical properties through a judicious spacer modification are currently under study in our laboratories with the aim of creating new materials for practical applications in the fields of sensing and magnetism.

ASSOCIATED CONTENT

Supporting Information

Further details are given in Figures S1–S17 and the crystallographic tables for **4**. This material is available free of charge via the Internet at <http://pubs.acs.org>. The crystallographic data for **4** have been deposited with the Cambridge Crystallographic Data Centre (CCDC Number 878230).

AUTHOR INFORMATION

Corresponding Author

*E-mail: a.rossin@iccom.cnr.it

Notes

The authors declare no competing financial interest.

ACKNOWLEDGMENTS

The *motu proprio* FIRENZE HYDROLAB project by Ente Cassa di Risparmio di Firenze (<http://www.iccom.cnr.it/hydrolab/>) is kindly acknowledged for funding this research activity. The authors also thank MATTM and DPM-CNR for financial support through the PIRODE and EFOR projects. The FP7-EU FREECATS project (NMP3-SL-2012-280658) is acknowledged for financial support. Dr. Gianluca Accorsi, researcher at Consiglio Nazionale delle Ricerche, Istituto per la Sintesi Organica e la Fotoreattività (ISOF-CNR)–Molecular Photoscience Group, is acknowledged for the photoluminescence measurements and data. We thank Prof. Andrea Caneschi for stimulating discussion. The financial support of the Italian MIUR through the PRIN 20097X44S7 (RECORD) Project and CNR through PM.P04.010 (MACOL) is also acknowledged.

REFERENCES

- (1) Armelao, L.; Quici, S.; Barigelletti, F.; Accorsi, G.; Bottaro, G.; Cavazzini, M.; Tondello, E. *Coord. Chem. Rev.* **2010**, *254*, 487–505.
- (2) (a) Quici, S.; Cavazzini, M.; Marzanni, G.; Accorsi, G.; Armaroli, N.; Ventura, B.; Barigelletti, F. *Inorg. Chem.* **2005**, *44*, 529–537. (b) Bünzli, J.-C.; G. *Acc. Chem. Res.* **2006**, *39*, 53–61.
- (3) Sabbatini, N.; Guardigli, M.; Lehn, J. M. *Coord. Chem. Rev.* **1993**, *123*, 201–228.
- (4) Armaroli, N.; Accorsi, G.; Barigelletti, F.; Couchman, S. S.; Fleming, J. S.; Harden, N. C.; Jeffery, J. C.; Mann, K. L. V.; McCleverty, J. A.; Rees, L. H.; Starling, S. R.; Ward, M. D. *Inorg. Chem.* **1999**, *38*, 5769–5776.
- (5) Herrera, J. M.; Pope, S. J. A.; Adams, H.; Faulkner, S.; Ward, M. D. *Inorg. Chem.* **2006**, *45*, 3895–3904.
- (6) Shi, D. L.; Lian, J.; Wang, W.; Liu, G. K.; He, P.; Dong, Z.; Wang, L. M.; Ewing, R. C. *Adv. Mater.* **2006**, *18*, 189–193.
- (7) (a) Zhang, H.-J.; Wang, X.-Z.; Zhu, D.-R.; Song, Y.; Xu, Y.; Xu, H.; Shen, X.; Gao, T.; Huang, M.-X. *CrystEngComm* **2011**, *13*, 2586–2592. (b) Feng, X.; Liu, B.; Wang, L.-Y.; Zhao, J.-S.; Wang, J.-G.; Weng, N. S.; Shi, X.-G. *Dalton Trans.* **2010**, *39*, 8038–8049. (c) Dai, F.; Cui, P.; Ye, F.; Sun, D. *Cryst. Growth Des.* **2010**, *10*, 1474–1477. (d) Zhao, B.; Chen, X. Y.; Chen, Z.; Shi, W.; Cheng, P.; Yan, S. P.; Liao, D. Z. *Chem. Commun.* **2009**, 3113–3115. (e) Klein, N.; Senkovska, I.; Gedrich, K.; Stoeck, U.; Henschel, A.; Mueller, U.; Kaskel, S. *Angew. Chem., Int. Ed.* **2009**, *48*, 9954–9957. (f) Cheng, A. L.; Ma, Y.; Zhang, J. Y.; Gao, E. Q. *Dalton Trans.* **2008**, 1993–2004. (g) MasPOCH, D.; Ruiz-Molina, D.; Veciana, J. *Chem. Soc. Rev.* **2007**, *36*, 770–818. (h) Mahata, P.; Sundaresan, A.; Natarajan, S. *Chem. Commun.* **2007**, 4471–4473. (i) Cheng, J.-W.; Zheng, S.-T.; Yang, G.-Y. *Dalton Trans.* **2007**, 4059–4066. (j) Zhu, W.-H.; Wang, Z.-M.; Gao, S. *Inorg. Chem.* **2007**, *46*, 1337–1342.
- (8) (a) Du, M.; Jiang, X. J.; Zhao, X. J. *Inorg. Chem.* **2007**, *46*, 3984–3985. (b) Lan, A. J.; Han, L.; Yuan, D. Q.; Jiang, F. L.; Hong, M. C. *Inorg. Chem. Commun.* **2007**, *10*, 993–996. (c) Wang, X.-L.; Bi, Y.-F.;

- Lin, H.-Y.; Liu, G.-C. *Cryst. Growth Des.* **2007**, *7*, 1086–1091. (d) Lu, Z.; Wen, L.; Ni, Z.; Li, Y.; Zhu, H.; Meng, Q. *Cryst. Growth Des.* **2007**, *7*, 268–274.
- (9) (a) Sonnauer, A.; Nather, C.; Hoppe, H. A.; Senker, J.; Stock, N. *Inorg. Chem.* **2007**, *46*, 9968–9974. (b) Gandara, F.; Garcia-Cortes, A.; Cascales, C.; Gomez-Lor, B.; Gutierrez-Puebla, E.; Iglesias, M.; Monge, A.; Snejko, N. *Inorg. Chem.* **2007**, *46*, 3475–3484. (c) Serre, C.; Millange, F.; Thouvenot, C.; Gardant, N.; Pellé, F.; Férey, G. *J. Mater. Chem.* **2004**, *14*, 1540–1543.
- (10) (a) de Lill, D. T.; de Bettencourt-Dias, A.; Cahill, C. L. *Inorg. Chem.* **2007**, *46*, 3960–3965. (b) McManus, G. J.; Perry, J. J.; Perry, M.; Wagner, B. D.; Zaworotko, M. J. *J. Am. Chem. Soc.* **2007**, *129*, 9094–9101. (c) Chen, B. L.; Yang, Y.; Zapata, F.; Qian, G. D.; Luo, Y. S.; Zhang, J. H.; Lobkovsky, E. B. *Inorg. Chem.* **2006**, *45*, 8882–8886. (d) Wagner, B. D.; McManus, G. J.; Moulton, B.; Zaworotko, M. J. *Chem. Commun.* **2002**, 2176–2177.
- (11) Kurmoo, M. *Chem. Soc. Rev.* **2009**, *38*, 1353–1379, and references therein.
- (12) Carlin, R. L. *Magnetochemistry*; Springer-Verlag: Berlin, Germany, 1986.
- (13) Gatteschi, D.; Sessoli, R.; Villain, J. *Molecular nanomagnets*; Oxford University Press: Oxford, U.K., 2006.
- (14) Ishikawa, N.; Sugita, M.; Ishikawa, T.; Koshihara, S.; Kaizu, Y. *J. Am. Chem. Soc.* **2003**, *125*, 8694–8695.
- (15) Bogani, L.; Sangregorio, C.; Sessoli, R.; Gatteschi, D. *Angew. Chem., Int. Ed.* **2005**, *44*, 5817–5821.
- (16) (a) Coulon, C.; H., M.; Clérac, R. *Struct. Bonding (Berlin, Ger.)* **2006**, *122*, 163–206. (b) Bogani, L.; Vindigni, A.; Sessoli, R.; Gatteschi, D. *J. Mater. Chem.* **2008**, *18*, 4750–4758.
- (17) Cornia, A.; Caneschi, A.; Dapporto, P.; Fabretti, A. C.; Gatteschi, D.; Malavasi, W.; Sangregorio, C.; Sessoli, R. *Angew. Chem., Int. Ed.* **1999**, *38*, 1780–1782.
- (18) (a) Rossin, A.; Ienco, A.; Costantino, F.; Montini, T.; Di Credico, B.; Caporali, M.; Gonsalvi, L.; Fornasiero, P.; Peruzzini, M. *Cryst. Growth Des.* **2008**, *8*, 3302–3308. (b) Rossin, A.; Fairen-Jimenez, D.; Düren, T.; Giambastiani, G.; Peruzzini, M.; Vitillo, G. *J. Langmuir* **2011**, *27*, 10124–10131.
- (19) *CrysAlis CCD 1.171.31.2 (release 07–07–2006)*, *CrysAlis171.NET*; Oxford Diffraction Ltd: Abingdon, U.K., 2006.
- (20) *CrysAlis RED 1.171.31.2 (release 07–07–2006)*, *CrysAlis171.NET*; Oxford Diffraction Ltd: Abingdon, U.K., 2006.
- (21) Altomare, A.; Burla, M. C.; Camalli, M.; Cascarano, G. L.; Giacovazzo, C.; Guagliardi, A.; Moliterni, A. G. G.; Polidori, G.; Spagna, R. *J. Appl. Crystallogr.* **1999**, *32*, 115–119.
- (22) Sheldrick, G. M. *SHELXL*; University of Göttingen: Göttingen, Germany, 1997.
- (23) Nardelli, M. *Comput. Chem.* **1993**, *7*, 95–98.
- (24) Farrugia, L. J. *J. Appl. Crystallogr.* **1997**, *30*, 565.
- (25) De Mello, J. C.; Wittmann, H. F.; Friend, R. H. *Adv. Mater.* **1997**, *9*, 230–232.
- (26) Rossin, A.; Chierotti, M. R.; Giambastiani, G.; Gobetto, R.; Peruzzini, M. *CrystEngComm* **2012**, DOI:10.1039/C2CE25048A.
- (27) (a) Alexandrov, E. V.; Blatov, V. A.; Kochetkov, A. V.; Proserpio, D. M. *CrystEngComm* **2011**, *13*, 3947–3958. (b) O’Keeffe, M.; Peskov, M. A.; Ramsden, S. J.; Yaghi, O. M. *Acc. Chem. Res.* **2008**, *41*, 1782–1789.
- (28) Blatov, V. A. *IUCr CompComm Newsletter* **2006**, *7*, 4–38 ; <http://www.topos.ssu.samara.ru>.
- (29) Li, M.; Liu, B.; Wang, B.; Wang, Z.; Gao, S.; Kurmoo, M. *Dalton Trans.* **2011**, *40*, 6038–6046.
- (30) Liu, B.; Zheng, H.-B.; Wang, Z.-M.; Gao, S. *CrystEngComm* **2011**, *13*, 5285–5288.
- (31) (a) Li, M.; Ako, A. M.; Lan, Y.; Wernsdorfer, W.; Buth, G.; Anson, C. E.; Powell, A. K.; Wang, Z.; Gao, S. *Dalton Trans.* **2010**, *39*, 3375–3377. (b) Cui, D.; Nishiura, M.; Tardif, O.; Hou, Z. *Organometallics* **2008**, *27*, 2426–2435. (c) Legendziewicz, J.; Glowiak, T.; Oczko, G.; Ngoan, D. C. *J. Less-Common Met.* **1986**, *125*, 45–57.
- (32) Anhydrous Gd(HCOO)₃ was prepared through the reaction between gadolinium(III) carbonate Gd₂(CO₃)₃ and an excess (ca. 2.5 equiv) of formic acid (98%) in water. The initial suspension slowly turns into a colorless solution while CO₂ gas evolves from the reaction flask. Subsequent water removal leaves a white crystalline residue of Gd(HCOO)₃ in a nearly quantitative yield.
- (33) Pabst, A. *J. Chem. Phys.* **1943**, *11*, 145–149.
- (34) Lin, J.-M.; Guan, Y.-F.; Wang, D.-Y.; Dong, W.; Wang, X.-T.; Gao, S. *Dalton Trans.* **2008**, 6165–6169.
- (35) Xu, Y.; Ding, S.-H.; Zhou, G.-P.; Liu, Y.-G. *Acta Crystallogr.* **2006**, *E62*, m1749–m1750.
- (36) Go, Y. B.; Jacobson, A. J. *Chem. Mater.* **2007**, *19*, 4702–4709.
- (37) Ushchapovskii, A. G.; Kashaev, A. A. *Kristallografiya* **1975**, *20*, 192.
- (38) Armelao, L.; Bottaro, G.; Quici, S.; Cavazzini, M.; Scalera, C.; Accorsi, G. *Dalton Trans.* **2011**, *40*, 11530–11538.
- (39) Ishii, A.; Kishi, S.; Ohtsu, H.; Iimori, T.; Nakabayashi, T.; Ohta, N.; Tamai, N.; Melnik, M.; Hasegawa, M.; Shigesato, Y. *ChemPhysChem* **2007**, *8*, 1345–1351.
- (40) Shekhah, O.; Liu, J.; Fischer, R. A.; Wöll, Ch. *Chem. Soc. Rev.* **2011**, *40*, 1081–1106.
- (41) Stein, G.; Würzberg, E. *J. Chem. Phys.* **1975**, *62*, 208–213.
- (42) Dong, D.-P.; Liu, L.; Sun, Z.-G.; Jiao, C.-Q.; Liu, Z.-M.; Li, C.; Zhu, Y.-Y.; Chen, K.; Wang, C.-L. *Cryst. Growth Des.* **2011**, *11*, 5346–5354.
- (43) Orendáč, M.; Sedláková, L.; Čižmár, E.; Orendáčová, A.; Feher, A.; Zvyagin, S. A.; Wosnitza, J.; Zhu, W. H.; Wang, Z. M.; Gao, S. *Phys. Rev. B* **2010**, *81*, 214410–214418.
- (44) Anderson, A. C.; Robichaux, J. E. *Phys. Rev. B* **1971**, *3*, 1410–1417.
- (45) (a) Sessoli, R. *Angew. Chem., Int. Ed.* **2012**, *51*, 43–45. (b) Evangelisti, M.; Roubeau, O.; Palacios, E.; Camon, A.; Hooper, T. N.; Brechin, E. K.; Alonso, J. J. *Angew. Chem., Int. Ed.* **2011**, *50*, 6606–6609. (c) Evangelisti, M.; Brechin, E. K. *Dalton Trans.* **2010**, *39*, 4672–4676.
- (46) Sedlakova, L.; Hanco, J.; Orendacova, A.; Orendac, M.; Zhou, C. L.; Zhu, W. H.; Wang, B. W.; Wang, Z. M.; Gao, S. *J. Alloys Compd.* **2009**, *487*, 425–429.